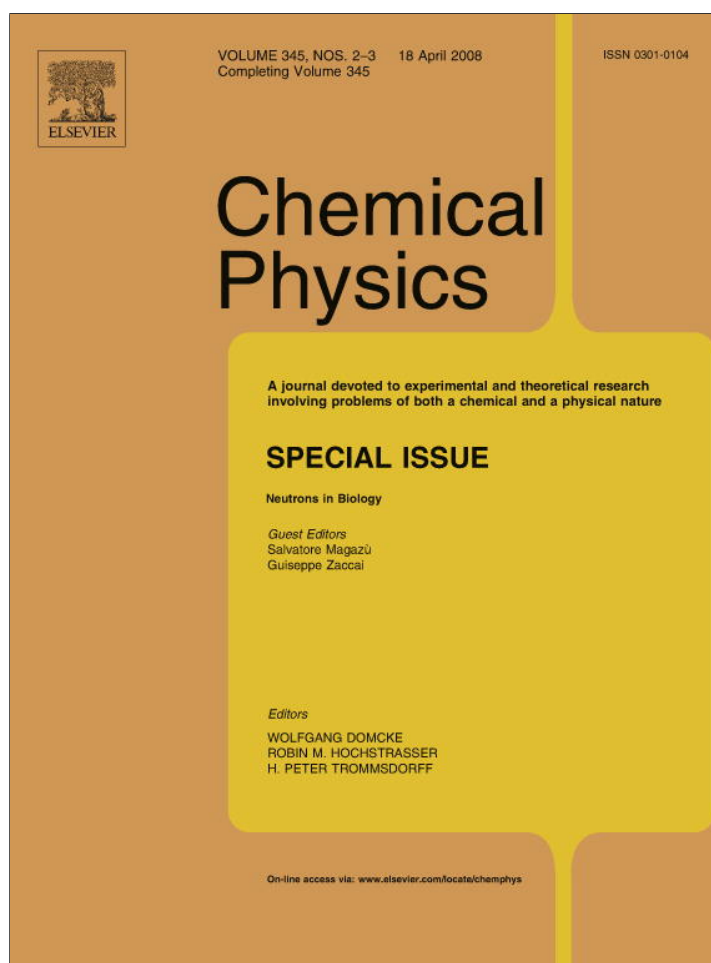


Provided for non-commercial research and education use.  
Not for reproduction, distribution or commercial use.



This article appeared in a journal published by Elsevier. The attached copy is furnished to the author for internal non-commercial research and education use, including for instruction at the authors institution and sharing with colleagues.

Other uses, including reproduction and distribution, or selling or licensing copies, or posting to personal, institutional or third party websites are prohibited.

In most cases authors are permitted to post their version of the article (e.g. in Word or Tex form) to their personal website or institutional repository. Authors requiring further information regarding Elsevier's archiving and manuscript policies are encouraged to visit:

<http://www.elsevier.com/copyright>



# Relaxation dynamics of lysozyme in solution under pressure: Combining molecular dynamics simulations and quasielastic neutron scattering

V. Calandrini<sup>a,b</sup>, V. Hamon<sup>a</sup>, K. Hinsén<sup>a,b</sup>, P. Calligari<sup>a,c,d</sup>,  
M.-C. Bellissent-Funel<sup>d</sup>, G.R. Kneller<sup>a,b,\*</sup>

<sup>a</sup> Centre de Biophysique Moléculaire, Rue Charles Sadron, 45071 Orléans, France

<sup>b</sup> Synchrotron Soleil, L'Orme de Merisiers, B.P. 48, 91192 Gif-sur-Yvette, France

<sup>c</sup> Institut Laue-Langevin, 6 Rue Jules Horowitz, B.P. 156, 38042 Grenoble, France

<sup>d</sup> Laboratoire Léon Brillouin, CEA Saclay, 91191 Gif-sur-Yvette, France

Received 11 May 2007; accepted 12 July 2007

Available online 25 July 2007

## Abstract

This paper presents a study of the influence of non-denaturing hydrostatic pressure on the relaxation dynamics of lysozyme in solution, which combines molecular dynamics simulations and quasielastic neutron scattering experiments. We compare results obtained at ambient pressure and at 3 kbar. Experiments have been performed at pD 4.6 and at a protein concentration of 60 mg/ml. For both pressures we checked the monodispersity of the protein solution by small angle neutron scattering. To interpret the simulation results and the experimental data, we adopt the fractional Ornstein–Uhlenbeck process as a model for the internal relaxation dynamics of the protein. On the experimental side, global protein motions are accounted for by the model of free translational diffusion, neglecting the much slower rotational diffusion. We find that the protein dynamics in the observed time window from about 1 to 100 ps is slowed down under pressure, while its fractal characteristics is preserved, and that the amplitudes of the motions are reduced by about 20%. The slowing down of the relaxation is reduced with increasing  $q$ -values, where more localized motions are seen.

© 2007 Published by Elsevier B.V.

**Keywords:** Protein dynamics; Quasielastic neutron scattering; Slow relaxation; Fractional Brownian dynamics

## 1. Introduction

In the last decades many studies have been devoted to the influence of pressure on the structure of proteins, which can be considered as the building blocks of living matter. One of the motivations is to understand the adaptation of living organisms to extreme thermodynamic conditions, as they occur for example at the deep sea level, where pressures up to several hundred bars must be sustained. Prob-

ably the first published study of proteins under pressure goes back to 1914, when Bridgman observed that exerting pressure on egg white has a similar effect as boiling it [1]. A recent review on the topic can be found in [2]. From a thermodynamic point of view, the extensive conjugate variable related to pressure is the volume and changing the pressure exerted on a system permits a fine-tuned exploration of its energy landscape through small volume changes. Particularly interesting in this context is the study of biological macromolecules by high pressure X-ray crystallography, which yields high resolution atomic structures and permits thus to relate energetic changes of these molecules to conformational changes [3]. This aspect plays a fundamental role in medical research, since the relation between pressure

\* Corresponding author. Address: Centre de Biophysique Moléculaire, Rue Charles Sadron, 45071 Orléans, France.

E-mail address: [kneller@cnrs-orleans.fr](mailto:kneller@cnrs-orleans.fr) (G.R. Kneller).

and the energy landscape affects amyloid fibril formation, which is typical for diseases like Alzheimer and the Creutzfeld–Jacob syndrome [4]. In the vast majority of experiments which have been performed in the past, the temperature has been used as a parameter to steer the exploration of the energy landscape via entropy changes. In this context we refer to neutron scattering studies of the dynamical transition, which is seen in many proteins at temperatures of about 200 K [5] and which manifests itself through an increase of the amplitudes of motions seen in these experiments.

In this work we study the influence of pressure on the internal dynamics of lysozyme in solution, using molecular dynamics (MD) simulations and quasielastic neutron scattering (QENS) experiments. Concerning structural changes under pressure, lysozyme has been studied in the past by X-ray crystallography in the pioneering work of Kundrot and Richards [6] and more recently by NMR by Refae et al. [7]. As for the simulations and the experiments, the work is based on the thesis work of Hamon [8]. The paper is organized as follows: In Section 2 the QENS experiments and the simulations are briefly described and Section 3 contains an introduction of the model we used for the analysis of the simulations and of the experiments. Section 4 describes the analyses of the simulations and of the experimental data, which is followed by a presentation of the results. The paper is concluded in Section 5 by a short résumé.

## 2. Materials and methods

### 2.1. Experiments

We prepared deuterated solutions of lysozyme at a concentration of 60 mg/ml and a pD of 4.6. The protein was purchased in powder form and was dissolved in a deuterated sodium acetate buffer at a concentration of 50 mM. All labile hydrogen atoms in lysozyme were exchanged by dialysis during three days, and the final solution was centrifuged to eliminate possible aggregates. The concentration of 60 mg/ml was chosen as a compromise between the necessity to use a maximum concentration for the neutron scattering experiments and to avoid, on the other hand, aggregation of the lysozyme molecules. Under the conditions described above lysozyme has a positive charge of about 11e, and small angle neutron scattering experiments have shown that the solution is monodisperse up to 100 mg/ml [9]. In this context we also quote dynamic light scattering experiments on lysozyme in solution under pressure, where a concentration of 80 mg/ml was used to measure the diffusion coefficient of lysozyme [10]. These experiments have been performed in a hydrogenated buffer, where the lysozyme–lysozyme interactions are less attractive than in the corresponding deuterated buffers [9] and the tendency to form aggregates is thus reduced. We checked, however, by a short run on a small angle neutron scattering spectrometer that aggregation did not occur – neither at ambient pressure, nor at high pressure.

The QENS experiments presented in this article were performed on the time-of-flight spectrometer IN5 at the Institut Laue-Langevin in Grenoble. The neutron spectra were measured with an incident neutron wavelength of  $\lambda = 5 \text{ \AA}$  corresponding to an elastic  $q$ -range of  $0.3\text{--}2.3 \text{ \AA}^{-1}$ . The elastic energy resolution determined by vanadium standard runs was  $\Delta E = 0.060 \text{ meV}$  (half width half maximum). Experiments have been performed at room temperature on both the lysozyme solution and the deuterated buffer at ambient pressure and at a pressure of 3 kbar. Buffer runs are used to evaluate the solvent contribution in the solution runs in order to isolate the contribution arising from the protein alone. For the given protein concentration of 60 mg/ml, the volume fraction of the protein and its first hydration shell can be estimated as 0.06, and the remaining fraction of 0.94 corresponds thus to the bulk solvent. This shows that the measured signal is dominated by scattering from the deuterated solvent, and that the incoherent scattering from the hydrogenated protein is very small, despite the large incoherent cross section of the hydrogen atoms. The subtraction of the solvent contribution has thus to be performed carefully. We used a pressure cell made of a ‘null alloy’ of 34% titanium and 66% zirconium, which was conceived to carry out earlier experiments on liquid heavy water [11]. Using the above composition the mean coherent scattering length is zero, the coherent scattering lengths of Ti and Zr atoms having opposite signs (see Table 1), and the cell scatters thus only incoherently. The null alloy has been elaborated by the manufacture of CEZUS (Compagnie européenne du zirconium, Ugine, Savoie), France where tests of mechanical resistance have been performed. Table 2 gives the mechanical characteristics of the alloy. The cell has cylindrical geometry and its dimensions (internal diameter = 5.7 mm, wall thickness = 5.2 mm) have been determined in order to withstand pressures up to 10 kbar. The cell was connected to the hydraulic pressurizing system via a capillary; the pressurizing

Table 1  
Characteristics of the null Ti–Zr alloy

	Ti	Zr
Coherent scattering length ( $10^{-12} \text{ cm}$ )	−0.3438	0.716
	Null alloy	
Composition	67 at.% (52 wt%)	33 at.% (48 wt%)
Scattering cross section (barn)	1.930	
Absorption cross section (barn) <sup>a</sup>	11.504	
Transmission linear coefficient ( $\text{cm}^{-1}$ ) <sup>a</sup>	0.697	

<sup>a</sup> Referred to  $\lambda = 5 \text{ \AA}$ .

Table 2  
Mechanical properties of the null Ti–Zr alloy from Ref. [11]

	$R_m$	923 MPa
Tensile strength	$R_m$	923 MPa
Yield point	$\sigma_{0.2}$	762 MPa
Elongation at the fracture	$A$	8%
Young modulus	$E$	85,000 MPa

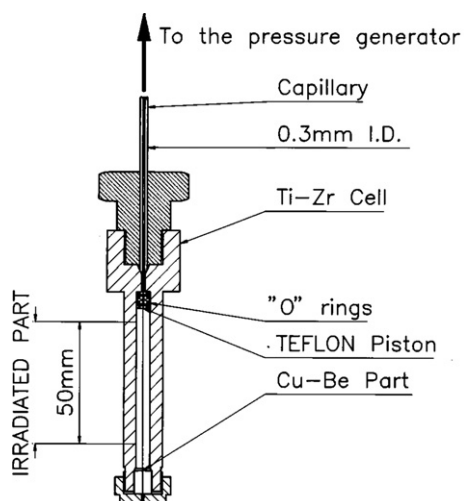


Fig. 1. Scheme of Ti-Zr high pressure cell.

medium was heavy water which was isolated from the sample by a Teflon piston (see Fig. 1). The strong scattering by the pressure cell was corrected for. Moreover, QENS data were corrected for detector efficiency, normalized to the integrated vanadium intensity, converted to the energy scale as well as converted from constant scattering angle  $\theta$  to constant momentum transfer  $q$ .

## 2.2. Simulations

The simulated system consists of one lysozyme molecule and 3403  $\text{H}_2\text{O}$  molecules in a box of dimensions  $6.15 \times 4.10 \times 4.61 \text{ nm}^3$ . The protein structure was taken from the Brookhaven protein databank [12] (code 193L [13]), to which the hydrogen atoms were added according to standard criteria concerning the chemical bond structure of amino acids. This leads to 1960 atoms for the lysozyme molecule and to 12,169 atoms in total for the simulated system. All simulations have been performed in the thermodynamic  $NpT$ -ensemble, using the program package MMTK [14] with the AMBER94 force field [15] for molecular simulations of proteins. Within the AMBER force field the  $\text{H}_2\text{O}$  molecules are modeled by the TIP3P potential. Since we were not interested in the solvent dynamics, we avoided the adaptation of the TIP3P potential to model heavy water, which was used in the experiments, and simulated light water instead. We note that only the dynamics of the slow, large amplitude motions of a protein is influenced by the solvent [16], and one can consider that it is essentially the viscosity of the solvent which has a major effect in this context. Since the viscosities of light and heavy water are similar, the replacement  $\text{D}_2\text{O} \rightarrow \text{H}_2\text{O}$  in the simulation is thus justified.

The long-range electrostatic forces and energies have been computed with a modified Ewald summation procedure [17]. In contrast to the experimental conditions, where each lysozyme molecule carries a charge of  $11e$  (pD 4.6), the simulated lysozyme molecule was kept neutral to ensure global neutrality of the simulated system. This is necessary

because the system is too small to model protein–protein interactions and the buffer realistically. The trajectories used for this article have been recorded with a sampling step of  $\Delta t = 0.04 \text{ ps}$ . The water trajectories were not stored and for subsequent analyses global translations and rotations of the simulated lysozyme molecule have been filtered out by performing for each sampling time step an optimal superposition of the molecular structure with the corresponding initial structure [18]. The generated trajectories thus describe only the internal dynamics of the simulated lysozyme molecule.

## 3. A simple model for protein dynamics

To interpret both the simulated and experimental data, we use the fractional Ornstein–Uhlenbeck (OU) process [19] as an analytical model for the atomic motions in a protein. The model describes anomalous diffusion in a harmonic potential, where the latter accounts for the fact that atomic motions in a protein are confined in space. The anomalous diffusion describes slow, non-exponential structural relaxation in the functional dynamics of proteins, which has been observed in the past on the microsecond to second time scale by fluorescence correlation spectroscopy [20] and by kinetic studies [21]. The existence of fractional Brownian dynamics in proteins on the nanosecond time scale has been recently demonstrated by analyses of molecular dynamics simulations [22] and the fractional OU process has been introduced in [23] for the interpretation of QENS spectra from proteins. It can be considered as an extension of a simple harmonic protein model, which has been used in the past to describe elastic neutron scattering profiles, in particular to extract the “resilience” of the protein under consideration in terms of an average force constant [24]. The fractional OU process adds to this a description of the relaxation dynamics, which is measured in QENS experiments.

### 3.1. Time-dependent mean-square displacement

The most elementary quantity to be considered in the context of diffusion processes is the time-dependent mean-square displacement (MSD),

$$W(t) := \langle [x(t) - x(0)]^2 \rangle, \quad (1)$$

where  $x$  is the position of the diffusing particle and the brackets indicate a thermal average. In case that the dynamics of the particle is confined in space, the MSD will tend to a plateau value, which is given by  $2\langle x^2 \rangle$ . This follows simply from definition (1), assuming a stationary stochastic process, such that  $W(t) = 2(\langle x^2 \rangle - \langle x(t)x(0) \rangle)$ , where  $\langle x^2 \rangle$  is finite due to the confinement. Using that any position autocorrelation function  $\langle x(t)x(0) \rangle$  tends to zero for  $t \rightarrow \infty$ , one obtains thus  $\lim_{t \rightarrow \infty} W(t) = 2\langle x^2 \rangle$ . For the fractional OU process one has

$$\langle x(t)x(0) \rangle = \langle x^2 \rangle E_\alpha(-[t/\tau]^\alpha), \quad 0 < \alpha \leq 1, \quad (2)$$

and the MSD takes the form

$$W(t) = 2\langle x^2 \rangle (1 - E_\alpha(-[t/\tau]^\alpha)). \quad (3)$$

Here  $E_\alpha(z)$  is the Mittag-Leffler function [25]

$$E_\alpha(z) = \sum_{k=0}^{\infty} \frac{z^k}{\Gamma(1 + \alpha k)}, \quad (4)$$

where  $\Gamma(\cdot)$  denotes the generalized factorial [26]. One recognizes that for  $\alpha = 1$ , where  $\Gamma(1 + \alpha k) = \Gamma(1 + k) = k!$ , the exponential function is retrieved from expression (4), i.e.  $E_1(z) = \exp(z)$ . In this case the fractional OU process becomes the well-known Markovian OU process [27–29]. As indicated in [23], the fractional counterpart is characterized by non-Markovian memory effects, which lead to non-exponential correlation functions.

Expressions (2) and (3) show that the proposed model contains three parameters:

- (1) the position fluctuation  $\langle x^2 \rangle$ ,
- (2) the parameter  $\alpha$  indicating the deviation from Markovian behavior,
- (3) the time scale parameter  $\tau$ .

### 3.2. Relaxation rate spectrum

The function  $E_\alpha(-[t/\tau]^\alpha)$  appearing in (2) and (3) can be considered as a “stretched” *generalized* exponential function. The non-exponential character of this function can be most easily visualized by writing it as a superposition of normal exponential functions. Using for simplicity a dimensionless time variable we have

$$E_\alpha(-t^\alpha) = \int_0^\infty d\lambda p_\alpha(\lambda) \exp(-\lambda t), \quad (5)$$

where  $p_\alpha(\lambda)$  is a normalized and positive distribution function, which is of the form [21,23]

$$p_\alpha(\lambda) = \frac{1}{\pi} \frac{\lambda^{\alpha-1} \sin(\pi\alpha)}{\lambda^{2\alpha} + 2\lambda^\alpha \cos(\pi\alpha) + 1}, \quad 0 < \alpha < 1. \quad (6)$$

In the limit  $\alpha \rightarrow 1$  we have [23]

$$\lim_{\alpha \rightarrow 1} p_\alpha(\lambda) = \delta(\lambda - 1), \quad (7)$$

in agreement with  $\lim_{\alpha \rightarrow 1} E_\alpha(-t^\alpha) = \exp(-t)$ .

### 3.3. Modeling incoherent neutron scattering

We consider in the following the dynamic structure factor for incoherent neutron scattering:

$$S(q, \omega) = \frac{1}{2\pi} \int_{-\infty}^{+\infty} dt \exp(-i\omega t) I(q, t), \quad (8)$$

where  $I(q, t)$  is the incoherent intermediate scattering function, which depends on the position of the scattering atom

$$I(q, t) = \langle \exp(iq[x(t) - x(0)]) \rangle. \quad (9)$$

Here  $q = |\mathbf{q}|$  is the modulus of the momentum transfer which the neutron transfers to scattering atom in the scattering process. Within the model we assume that the system under consideration is isotropic and that the protein dynamics, which is seen in incoherent neutron scattering, can be described by one “representative” atom. In this case it suffices to consider one coordinate of the scattering atom, which is chosen to be the  $x$ -coordinate. In view of the predominance of incoherent scattering by hydrogen atoms, the representative atom in the model is a representative hydrogen atom.

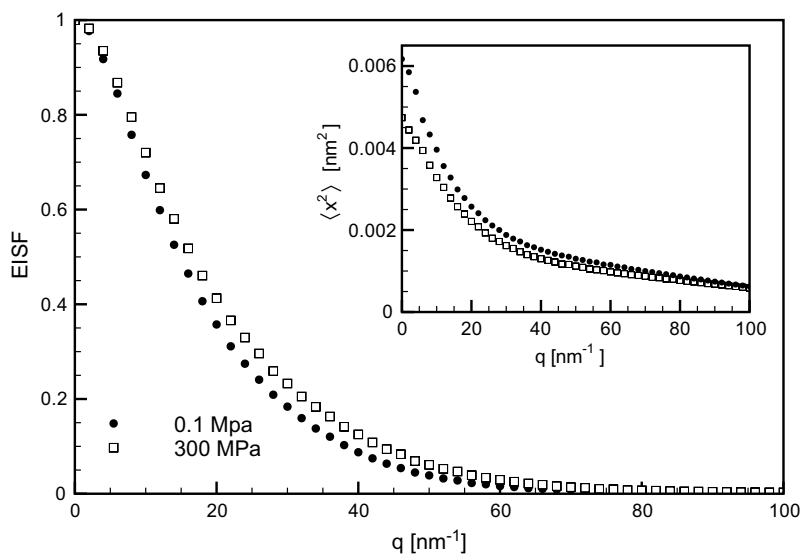


Fig. 2. Simulated EISF of lysozyme for  $p = 0.1$  MPa (bullets) and  $p = 300$  MPa (squares). The inset shows the position fluctuations derived from expression (13).

Within the model the intermediate scattering function has the form

$$I(q, t) = \exp(-q^2 \langle x^2 \rangle) \sum_{n=0}^{\infty} \frac{q^{2n} \langle x^2 \rangle^n}{n!} E_{\alpha}(-[t/\tau_n]^{\alpha}), \quad 0 < \alpha \leq 1, \quad (10)$$

where  $\tau_n$  is given by

$$\tau_n = \tau n^{-1/\alpha}. \quad (11)$$

Static correlation functions obtained from the model are the same as for the standard OU process. In the context of neutron scattering this concerns the elastic incoherent structure factor (EISF),

$$\text{EISF}(q) = \lim_{t \rightarrow \infty} I(q, t) = \exp(-q^2 \langle x^2 \rangle), \quad (12)$$

which has Gaussian form. In reality the Gaussian approximation holds strictly only for  $q \rightarrow 0$  [30]. Calculating  $\langle x^2 \rangle$  via

$$\langle x^2 \rangle = -\ln(\text{EISF}[q])/q^2 \quad (13)$$

one obtains a strongly  $q$ -dependent position fluctuation. Fig. 2 illustrates this aspect. Therefore, in the following  $\langle x^2 \rangle$ , as well as the parameters  $\alpha$  and  $\tau$  of the fractional OU process are considered  $q$ -dependent.

The dynamic structure factor associated with the intermediate scattering function (10) reads

$$S(q, \omega) = \exp(-q^2 \langle x^2 \rangle) \left\{ \delta(\omega) + \sum_{n=1}^{\infty} \frac{q^{2n} \langle x^2 \rangle^n}{n! 2\pi} L_{\alpha, \tau_n}(\omega) \right\}, \quad (14)$$

where  $L_{\alpha, \tau}(\cdot)$  is the generalized Lorentzian [22]

$$L_{\alpha, \tau}(\omega) = \frac{2\tau \sin(\alpha\pi/2)}{\omega\tau((\omega\tau)^{\alpha} + 2\cos(\alpha\pi/2) + (\omega\tau)^{-\alpha})}, \quad 0 < \alpha \leq 1. \quad (15)$$

## 4. Data analysis and results

### 4.1. Fitting simulated time correlation functions

The “natural” quantities for the analysis of MD simulations are MSDs and time correlation functions, which can be directly computed from the trajectories. In the present study we used the MD analysis package nMoldyn for this purpose [31]. To fit expressions (3) or (10) to the corresponding simulated functions one needs thus to evaluate functions of the type  $E_{\alpha}(-t^{\alpha})$ . We found the following procedure satisfactory. Starting from the decomposition (5) we perform the variable change  $u = \lambda^{\alpha}$  to obtain

$$E_{\alpha}(-t^{\alpha}) = \frac{1}{\pi\alpha} \int_0^{\infty} du \frac{\sin(\pi\alpha)}{u^2 + 2u \cos(\pi\alpha) + 1} \exp(-u^{1/\alpha} t), \quad (16)$$

where the integral is evaluated numerically. The variable change  $\lambda \rightarrow u$  leads to a well-behaved, non-singular inte-

grand and allows to compute  $E_{\alpha}(-t^{\alpha})$  for large arguments  $t$ , where the series expansion (4) converges extremely slowly. The method can be tested for the special case  $\alpha = 1/2$ , for which an analytical solution is known:  $E_{1/2}(-t^{1/2}) = \exp(t) \text{erfc}(\sqrt{t})$  [25].

### 4.2. Fitting QENS spectra

The model introduced in Section 3 describes internal protein dynamics and to be useful for the interpretation of QENS spectra of protein solutions the effects of global diffusion and of finite instrumental resolution must be incorporated. Neglecting multiple scattering effects and absorption, and assuming that global diffusion of the lysozyme molecules and internal motions are decoupled, we write the measured dynamic structure factor as convolution product (defining  $(f * g)(\omega) = \int_{-\infty}^{+\infty} d\omega' f(\omega - \omega') g(\omega')$ ):

$$S_m(q, t) = (S * l * r)(\omega). \quad (17)$$

Here  $S$  stands for the dynamic structure factor of the model,  $l$  is a Lorentzian describing translational diffusion ( $D$  is the diffusion constant),

$$l(\omega) = \frac{1}{\pi} \frac{Dq^2}{(Dq^2)^2 + \omega^2} \quad (18)$$

and  $r$  is the resolution function, which is well described by a Gaussian,

$$r(\omega) = \frac{\exp\left(-\frac{\omega^2}{2\sigma^2}\right)}{\sqrt{2\pi}\sigma}, \quad (19)$$

with  $\sigma > 0$  and a half width at half maximum (HWHM) of  $\Delta E \approx 1.17\sigma$ . Both  $r(\cdot)$  and  $l(\cdot)$  are normalized such that  $\int_{-\infty}^{+\infty} d\omega r(\omega) = 1$  and  $\int_{-\infty}^{+\infty} d\omega l(\omega) = 1$ .

From light scattering experiments one can estimate the relevance of translational diffusion for QENS spectra. In the work of Nystrom and Roots [10], which has been performed in similar conditions, the diffusion coefficient at  $p = 0.1$  MPa and  $p = 300$  MPa is found to be  $D = 1.45 \times 10^{-4}$  nm<sup>2</sup>/ps and  $D = 1.25 \times 10^{-4}$  nm<sup>2</sup>/ps, respectively. The width of the corresponding Lorentzian being  $Dq^2$ , we obtain for  $q = 20$  nm<sup>-1</sup> and  $p = 0.1$  MPa a width  $Dq^2 = 0.038$  meV, which is comparable to the instrumental resolution. To estimate the influence of rotational diffusion on the measured QENS spectra we use the diffusion constant for rotational diffusion [32], assuming that the protein under consideration has spherical shape,

$$\gamma_r = \frac{k_B T}{4\pi\eta a^3}. \quad (20)$$

Here  $a$  is the radius of the protein and  $\eta$  is the shear viscosity of the solvent (water). For lysozyme, which has a radius of  $a = 1.45$  nm, one obtains  $\gamma_r = 1.06 \times 10^8$  s<sup>-1</sup> at  $T = 293$  K. This corresponds to a width of  $7 \times 10^{-5}$  meV, which is far below the instrumental resolution. Rotational diffusion needs therefore not be considered in the model.

The convolution product (17) for the measured dynamics structure factor can be written in the following form, using  $S$  as the model (14),

$$S_m(q, \omega) = \exp(-q^2 \langle x^2 \rangle) \times \left\{ (I * r) + \sum_{n=1}^{\infty} \frac{q^{2n} \langle x^2 \rangle^n}{n! 2\pi} (L_{\alpha, \tau}^D * r)(\omega) \right\}. \quad (21)$$

Here  $L_{\alpha, \tau}^D(\omega) = (L_{\alpha, \tau} * I)(\omega)$  is the convolution of a generalized Lorentzian with a normal Lorentzian, for which an analytical form can be given. Defining

$$\tilde{\omega} = \sqrt{\omega^2 + (Dq^2)^2}, \quad \phi = \arg(Dq^2 + i\omega), \quad (22)$$

one obtains [33]

$$L_{\alpha, \tau}^D(\omega) = \frac{2\{(\tilde{\omega}\tau)^\alpha \cos \phi + \cos([\alpha - 1]\phi)\}}{\tilde{\omega}\{(\tilde{\omega}\tau)^\alpha + 2 \cos \alpha \phi + (\tilde{\omega}\tau)^{-\alpha}\}}. \quad (23)$$

In contrast to  $L_{\alpha, \tau}$ , its convolution with a normal Lorentzian stays finite at  $\omega = 0$  if  $D > 0$ . This point is important if one aims at evaluating the convolutions in (21) by the efficient Fast Fourier Transform technique [34], as we did for the fits presented in this article. With this method singular functions cannot be treated and we refer to [33] to handle the case of  $D = 0$ . It is worthwhile mentioning that the latter method can be easily generalized to include also global diffusion, but the FFT technique is more efficient.

### 4.3. Results

We start the presentation of the results with the analysis of the MD simulations. The most basic quantity to consider is the time-dependent mean-square displacement. Fig. 3 shows the neutron-weighted average atomic MSD of lysozyme and the fit of the model function (3). The atomic weights are chosen to be the squared incoherent

scattering lengths. We note that the MSD computed from MD is the sum of the MSDs in the  $x$ -,  $y$ - and  $z$ -direction, and expression (3) must thus be multiplied by 3 for the fit. In the latter only two of the three parameters of the model,  $\tau$  and  $\alpha$ , were used and the mean square position fluctuation  $\langle x^2 \rangle$  has been fixed by a separate analysis of the MD trajectory. The resulting fit parameters can be read off from Table 3. It is important to emphasize that the model parameters are quite strongly correlated, in particular  $\langle x^2 \rangle$  and  $\tau$ . Therefore a good estimation of  $\langle x^2 \rangle$  is crucial even to estimate tendencies of  $\tau$  with pressure. In this context we found that the direct calculation of  $\langle x^2 \rangle$  from the MD trajectories is less reliable than the calculation from the EISF via expression (13) in the limit  $q \rightarrow 0$ . For ambient pressure this procedure gives a very similar result as the direct calculation, but for  $p = 300$  MPa the direct calculation yields a value which is about 10% smaller than the one obtained from the EISF. This small difference leads even to a slight shortening of  $\tau$  with pressure instead to the lengthening seen in Table 3, and the fit is clearly less good. If all parameters are left free in the fit, one also finds a lengthening of  $\tau$  with pressure, and the resulting para-

Table 3  
Parameters for the fractional Ornstein–Uhlenbeck process obtained from fits to the simulated MSDs and to the simulated intermediate scattering functions

	0.1 MPa			300 MPa		
	$\langle x^2 \rangle$ (nm <sup>2</sup> )	$\alpha$	$\tau$ (ps)	$\langle x^2 \rangle$ (nm <sup>2</sup> )	$\alpha$	$\tau$ (ps)
MSD	$6.17 \times 10^{-3}$	0.54	31.75	$4.74 \times 10^{-3}$	0.54	39.08
$F_{\text{inc}}(6 \text{ nm}, t)$	$4.68 \times 10^{-3}$	0.53	13.48	$3.94 \times 10^{-3}$	0.50	19.43
$F_{\text{inc}}(10 \text{ nm}, t)$	$3.96 \times 10^{-3}$	0.51	8.86	$3.28 \times 10^{-3}$	0.49	13.58
$F_{\text{inc}}(20 \text{ nm}, t)$	$2.57 \times 10^{-3}$	0.52	2.53	$2.21 \times 10^{-3}$	0.45	4.39
$F_{\text{inc}}(22 \text{ nm}, t)$	$2.41 \times 10^{-3}$	0.50	2.3	$2.08 \times 10^{-3}$	0.44	3.64

The value of  $\langle x^2 \rangle$  is fixed according to Eq. (13).

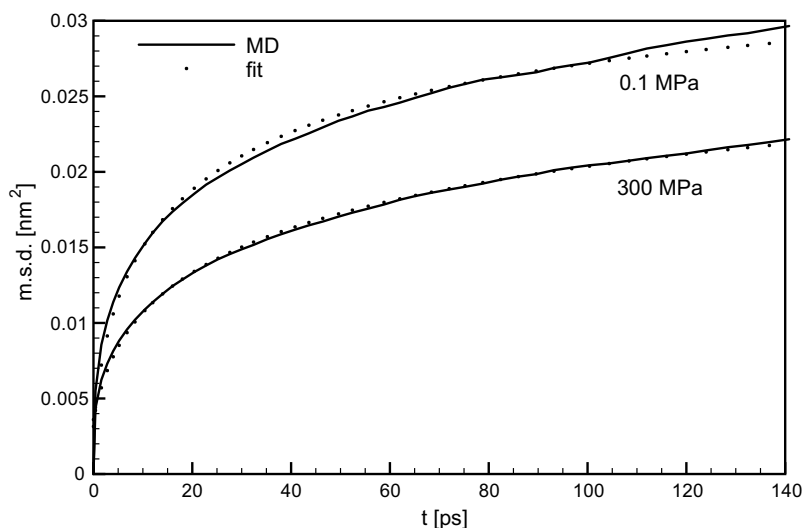


Fig. 3. Average atomic mean-square displacement of lysozyme in solution obtained from MD simulation at  $p = 0.1$  MPa and at  $p = 300$  MPa (solid lines). The broken lines correspond to a fit of the model according to expression (3). See Table 3 for the resulting parameters. More explanations are given in the text.

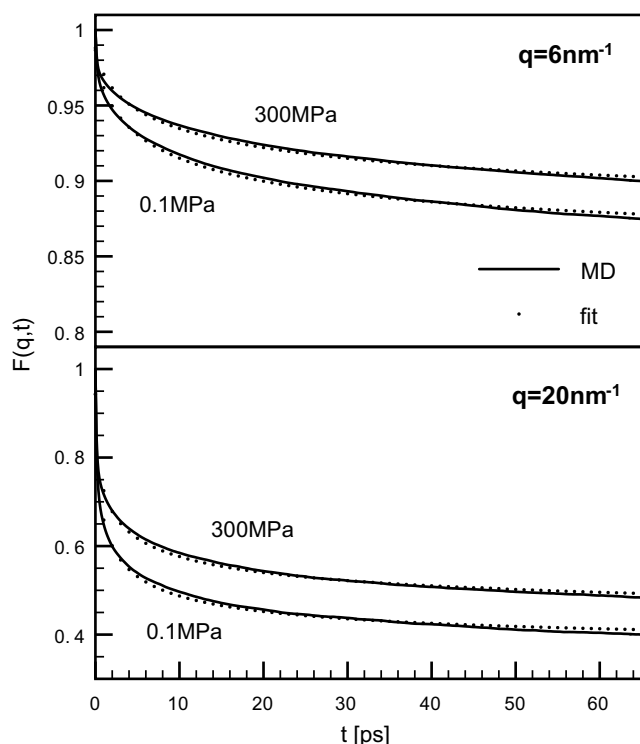


Fig. 4. Fit of the simulated incoherent dynamic structure factor (solid lines) with expression (10) (broken lines) for  $p = 0.1$  MPa (upper part) and  $p = 300$  MPa (lower part). The parameters are given in Table 3.

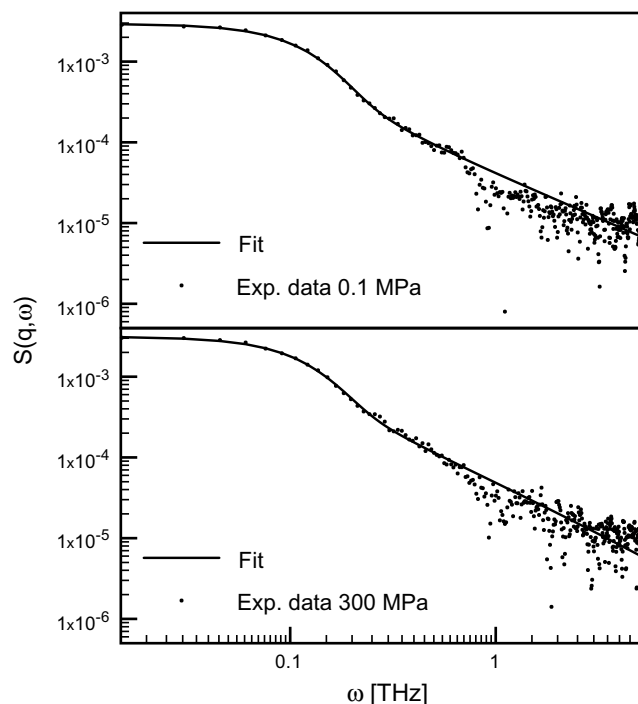


Fig. 5. Log-log plot of experimental QENS spectra for  $q = 20$  nm<sup>-1</sup> (bullets) at ambient pressure (top) and at  $p = 300$  MPa (bottom) as a function of  $\omega$  (angular frequency). The solid lines represent the fits of the analytical model defined in Eq. (14) using the parameters given in Table 4.

eters are very similar to the ones found by imposing  $\langle x^2 \rangle$  obtained from the EISF. In view of these findings the fitted values for  $\alpha$  and  $\tau$  for the MSD at  $p = 300$  MPa, which have been published in [35], must be considered erroneous.

Fig. 4 shows the intermediate scattering function and the fitted model for  $q = 6$  nm<sup>-1</sup> and  $q = 20$  nm<sup>-1</sup> for the two pressures of  $p = 0.1$  MPa and  $p = 300$  MPa, respectively. The corresponding model parameters are listed in Table 3. The fits were performed with expression (10), using eight terms in the sum. As already indicated,  $I(q, t)$  has been fitted by using the  $q$ -dependent position fluctuations shown in Fig. 2.

Fig. 5 displays experimental QENS spectra at  $q = 20$  nm<sup>-1</sup> and the corresponding fit of expression (21), which accounts for finite instrumental resolution and for free translational diffusion of the lysozyme molecules in the solution. As for the fits of the simulated intermediate scattering functions, the position fluctuations have been read off from Fig. 2. The fit parameters  $\alpha$ ,  $\tau$  and the diffusion coefficient  $D$  are given in Table 4 for two  $q$ -values:

Table 4

Parameters obtained from a fit of expression (21) to the experimental QENS spectra

		$S_{\text{inc}}(20 \text{ nm}^{-1}, \omega)$	$S_{\text{inc}}(22 \text{ nm}^{-1}, \omega)$
0.1 MPa	$\langle x^2 \rangle$ (nm <sup>2</sup> )	$2.57 \times 10^{-3}$	$2.41 \times 10^{-3}$
	$\alpha$	0.35(2)	0.40(2)
	$\tau$ (ps)	3(2)	3(1)
	$\bar{D}$ (nm <sup>2</sup> ps <sup>-1</sup> )	$0.53(3) \times 10^{-4}$	
300 MPa	$\langle x^2 \rangle$ (nm <sup>2</sup> )	$2.21 \times 10^{-3}$	$2.08 \times 10^{-3}$
	$\alpha$	0.52(1)	0.55(1)
	$\tau$ (ps)	5.2(2)	4.7(3)
	$\bar{D}$ (nm <sup>2</sup> ps <sup>-1</sup> )	$0.50(3) \times 10^{-4}$	

The value of  $\langle x^2 \rangle$  is fixed according to Eq. (13).

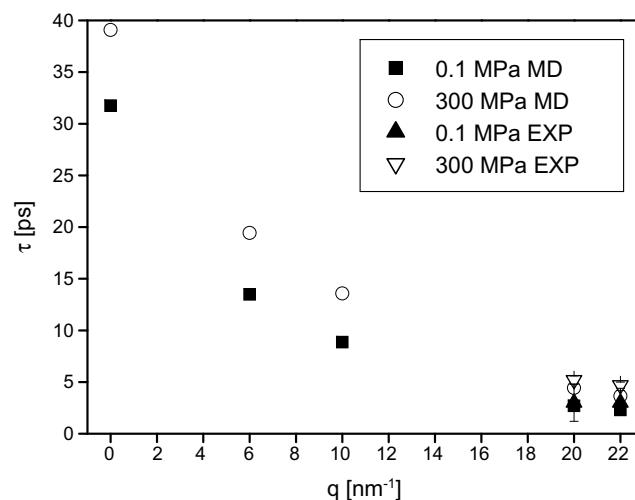


Fig. 6. Fitted model parameter  $\tau$  as a function of  $q$  for  $p = 0.1$  MPa and  $p = 300$  MPa. The black squares and the circles correspond to the analysis of the MD data at 0.1 MPa and at 300 MPa, respectively. The black and white triangles correspond to the fits to the experimental QENS spectra.

$q = 20 \text{ nm}^{-1}$  and  $q = 22 \text{ nm}^{-1}$ . For lower  $q$ -values the quasielastic signal was too small to be exploitable at the given resolution. The diffusion coefficients we find are about a factor of three smaller than what one would expect from quasielastic light scattering experiments.

The evolution of the time scale parameter  $\tau$  for both simulation results and QENS experiments is summarized in Fig. 6, where the values for  $q = 0$  correspond to the fits of the simulated mean-square displacements. One observes that the influence of pressure becomes less pronounced with increasing  $q$ , corresponding to increasingly localized motions.

## 5. Conclusion

In the present article we have studied the influence of pressure on the internal dynamics of lysozyme, using molecular dynamics simulations and quasielastic neutron scattering. The fractional Ornstein–Uhlenbeck process was used as a model to interpret both simulations and experiments, which were performed at ambient temperature and pressures of  $p = 0.1 \text{ MPa}$  and  $p = 300 \text{ MPa}$ . For both pressures, the analysis of the MSD and of the intermediate scattering functions obtained from MD simulation show that the relaxation time scale  $\tau$  decreases progressively with increasing  $q$ , while the parameter  $\alpha$ , which describes the fractal self-similarity of the observed relaxation dynamics, remains essentially constant at a value of  $\alpha = 0.5$ . This shows that the observed relaxation dynamics becomes increasingly faster the more localized the observed motions are, while the fractal characteristics of the dynamics is the same over all investigated spatial scales. We emphasize that the model parameters, which have been obtained from the QENS spectra at  $q = 20 \text{ nm}^{-1}$  and at  $q = 22 \text{ nm}^{-1}$  are in agreement with those obtained from the simulation data.

Concerning the effect of the pressure on both experimental QENS spectra and simulated quantities, we find that  $\alpha$  does not change with pressure either, indicating that pressure does not change the fractal behavior of the relaxation dynamics. It does, however, reduce the amplitude of the motions by about 20%, and it has an effect on the observed relaxation time scale. For all values of  $q$  pressure leads to an increase of  $\tau$ , thus indicating a systematic slowing down of the relaxation processes. This effect is the more pronounced the smaller  $q$  is, i.e. the larger the spatial scale of the relaxation dynamics is. This finding can be explained by an increase in the packing density of the atoms, which causes longer waiting times for large conformational rearrangements than for more localized rearrangements on the residue level, which are seen at higher  $q$ -values.

In order to obtain more insight into the relaxation mechanisms leading to the fractional Brownian motion observed protein dynamics, it is interesting to relate the present study to an analysis of a normal mode decomposition of the same trajectory [16]. The slowest relaxation time scales we find in this article are also observed in the dynam-

ics projected on the most collective modes, which is purely diffusive. On the other hand, the projection of the dynamics onto normal modes representing more localized motions also contains vibrational components. For this dynamical regime, fractional Brownian dynamics describes diffusive hopping processes between conformational substates, the relaxation time scale being the residence time in one of these substates.

## Acknowledgement

V. Calandrini acknowledges financial support by the Fondazione Angelo Della Riccia.

## References

- [1] P. Bridgman, Proc. Am. Acad. Arts Sci. 49 (1914) 627.
- [2] C. Balny, P. Masson, K. Heremans, Biochim. Biophys. Acta 1595 (1–2) (2002) 3.
- [3] R. Fourme, E. Girard, R. Kahn, A. Dhaussy, M. Mezouar, N. Colloc'h, I. Ascone, Biochim. Biophys. Acta 1764 (2006) 384.
- [4] F. Meersman, C. Dobson, K. Heremans, Chem. Soc. Rev. 35 (10) (2006) 908.
- [5] W. Doster, S. Cusack, W. Petry, Nature 337 (1989) 754.
- [6] C. Kundrot, F. Richards, J. Mol. Biol. 193 (1987) 157.
- [7] M. Refaee, T. Tezuka, K. Akasaka, M. Williamson, J. Mol. Biol. 327 (2003) 857.
- [8] V. Hamon, Influence de la pression sur la dynamique du lysozyme en solution, par simulation numérique et diffusion de neutrons, Ph.D. thesis, Université d'Orléans, 2004.
- [9] C. Gripon, L. Legrand, I. Rosenman, O. Vidal, M. Robert, F. Boué, J. Cryst. Growth 178 (1997) 575.
- [10] B. Nystrom, J. Roots, Makromol. Chem. 185 (1984) 1441.
- [11] M.-C. Bellissent-Funel, L. Bosio, J. Chem. Phys. 102 (9) (1995) 3727.
- [12] H. Berman, J. Westbrook, Z. Feng, G. Gilliland, T. Bhat, H. Weissig, I. Shindyalov, P. Bourne, Nucleic Acids Res. 28 (2000) 235.
- [13] M. Vaney, S. Maignan, M. RiesKautt, A. Ducruix, Acta Crystallogr., Sect D: Biol. Crystallogr. 52 (1996) 505.
- [14] K. Hinsen, J. Comput. Chem. 21 (2000) 79. <<http://dirac.cnrs-orleans.fr>>.
- [15] W. Cornell, P. Cieplak, C. Bayly, I.I.R. Gould, K. Merz Jr., D. Ferguson, D. Spellmeyer, T. Fox, J. Caldwell, P. Kollman, J. Am. Chem. Soc. 117 (1995) 5179.
- [16] K. Hinsen, G. Kneller, Proteins: Struct. Funct. and Bioinform., 2007, in press.
- [17] D. Wolf, P. Keblinski, S. Philpot, J. Eggebrecht, J. Chem. Phys. 110 (17) (1999) 8254.
- [18] G. Kneller, Mol. Simul. 7 (1991) 113.
- [19] R. Metzler, J. Klafter, Phys. Rep. 339 (2000) 1.
- [20] H. Yang, G. Luo, P. Karnchanaphanurach, T. Louie, I. Rech, S. Cova, L. Xun, X. Xie, Science 302 (5643) (2003) 262.
- [21] W. Glöckle, T. Nonnenmacher, Biophys. J. 68 (1995) 46.
- [22] G. Kneller, K. Hinsen, J. Chem. Phys. 121 (20) (2004) 10278.
- [23] G. Kneller, Phys. Chem. Chem. Phys. 7 (2005) 2641.
- [24] G. Zaccai, Science 288 (2000) 1604.
- [25] A. Erdélyi, W. Magnus, F. Oberhettinger, F. Tricomi, Higher Transcendental Functions, McGraw Hill, 1955.
- [26] M. Abramowitz, I. Stegun, Handbook of Mathematical Functions, Dover Publications, New York, 1972.
- [27] M. Wang, G. Uhlenbeck, Phys. Rev. 93 (1) (1945) 249.
- [28] C. Gardiner, Handbook of Stochastic Methods, second ed. Springer Series in Synergetics, Springer, Berlin, Heidelberg, New York, 1985.
- [29] H. Risken, The Fokker-Planck Equation, second ed. Springer Series in Synergetics, Springer, Berlin, Heidelberg, New York, 1996.

- [30] J. Boon, S. Yip, *Molecular Hydrodynamics*, McGraw Hill, 1980, see Eqs. (3.5.23), (3.5.33), (3.5.37) and the corresponding references.
- [31] T. Rog, K. Murzyn, K. Hinsén, G. Kneller, *J. Comput. Chem.* 24 (5) (2003) 657.
- [32] B. Cichocki, B. Felderhof, R. Schmitz, *PhysicoChem. Hydrodyn.* 10 (1988) 383.
- [33] G. Kneller, V. Calandrini, *J. Chem. Phys.* 126 (2007) 125107.
- [34] E. Brigham, *The Fast Fourier Transform*, Prentice Hall, 1974.
- [35] V. Hamon, P. Calligari, K. Hinsén, G. Kneller, *J. Non-Cryst. Solids* 352 (2006) 4417.